DOI: 10.1002/chem.200900584

Three-Component Langmuir–Blodgett Films Consisting of Surfactant, Clay Mineral, and Lysozyme: Construction and Characterization

Shiding Miao,[a] Hugo Leeman,[a] Steven De Feyter,[b] and Robert A. Schoonheydt*[a]

Abstract: The Langmuir–Blodgett (L–B) technique has been employed for the construction of hybrid films consisting of three components: surfactant, clay, and lysozyme (Lys). The surfactants are octadecylammonium chloride (ODAH) and octadecyl ester of rhodamine B (RhB18). The clays include saponite and laponite. Surface pressure versus area isotherms indicate that lysozyme is adsorbed by the surfactant–clay L–B film at the air–water interface without phase transition. The UV-visible spectra of the hybrid film ODAH–saponite–Lys show that the amount of immobilized lysozyme in the hybrid film is $(1.3\pm0.2)\,ng\,mm^{-2}$. The average surface area (Ω) per molecule of lysozyme is approximately $18.2\,nm^2$ in the saponite layer. For the multilayer film $(ODAH–saponite–Lys)_n$, the average amount of lysozyme per layer is $(1.0\pm0.1)\,ng\,mm^{-2}$. The amount of lysozyme found in the hybrid films of ODAH–laponite–Lys is at the detection limit of about $0.4\,ng\,mm^{-2}$. Attenuated total reflectance (ATR) FTIR spectra give evidence for clay layers, ODAH, lysozyme, and water in the hybrid film. The octadecylammonium cations are partially oxidized to the corresponding carbamate. A weak $1620\,cm^{-1}$ band of lysozyme in the hybrid films is reminiscent of the presence of lysozyme aggregates. AFM reveals evidence of randomly oriented saponite layers of various sizes and shapes. Individual lysozyme molecules are not resolved, but aggregates of about 20 nm in diameter are clearly seen. Some aggregates are in contact with the clay mineral layers, others are not. These aggregates are aligned in films deposited at a surface pressure of $20\,mN\,m^{-1}$.

Keywords: clays · interfaces · Langmuir–Blodgett films · lysozyme · surfactants

Introduction

Proteins are the most abundant macromolecules in cells and serve such functions as catalyzing chemical reactions (enzymes), regulating biological activity, transporting energy, oxygen and ions in biological processes, and so forth.[1] Generally, the use of protein solutions in chemical transformations is limited due to the poor stability and difficulty of separation.[2] Immobilization of enzymes or proteins on solid surfaces can partly overcome these limitations.[3] Therefore the interaction of proteins with solid surfaces is becoming a central problem of chemistry and biotechnology.[4] Much effort has been focused on immobilizing enzymes onto catalyst supports,[5] and preliminary results show that the composite catalyst has many advantages over the free enzyme, such as improved thermal and chemical stabilities,[6] enhanced catalytic activity due to a synergetic effect,[7] and ease of separation. In recent years there has been substantial interest in the field of supramolecular architecture with protein immobilization and formation of protein mono- and multilayers on solid surfaces.[8]

The Langmuir–Blodgett (L–B) technique is an elegant method for the transfer of monolayers from the air–water interface to a solid substrate.[9] Its application offers new possibilities in the production of advanced materials.[10] Up to now, L–B techniques have been widely used in preparing surfactants and protein monolayers with biomimetic purposes.[11] Many monolayers or hybrid multilayers including phospholipids,[12] enzymes,[13] and protein–lipid complexes[14] have been examined for L–B deposition. Compared with

[a] Dr. S. D. Miao, H. Leeman, Prof. R. A. Schoonheydt
Center for Surface Chemistry and Catalysis
Faculty of Bioscience Engineering
K.U. Leuven, Kasteelpark Arenberg 23
3001 Leuven (Belgium)
Fax: (+32) 16-321998
E-mail: Robert.Schoonheydt@biw.kuleuven.be

[b] Prof. S. De Feyter
Department of Chemistry, Division of
Photochemistry and Spectroscopy
K.U. Leuven, Celestijnenlaan 200-F
3001 Leuven (Belgium)

Supporting information for this article is available on the WWW under http://dx.doi.org/10.1002/chem.200900584.

other techniques, for example, Layer-by-Layer (L-b-L) assemblage,[15] the thickness of the layer and the molecular organization can be more precisely tailored according to a predesigned architecture by the L–B technique. However, it is difficult to build L–B films with prominent stability and integrity with proteins.[16] An alternative approach is to construct films of clay mineral layers and proteins. The clay layers are then the "bricks" in the reinforced multilayer assemblies.

Swelling clay minerals are silicates that consist of approximately 1 nm-thick layers, which are made of one sheet of edge-linked Al or Mg octahedra sandwiched between two sheets of corner-linked Si tetrahedra.[17] Isomorphous substitution occurs in the tetrahedral or octahedral sheets or in both. The negatively charged layers are compensated by exchangeable cations in the interlamellar space. In aqueous dispersion, additional water molecules are taken up in the interlamellar space. The clay mineral swells and the particles and aggregates fall apart into individual layers. These individual layers can be assembled in mono- and multilayers by the L–B technique, as reviewed by Schoonheydt et al.[18] Hybrid clay mineral–protein films can also be prepared by L-b-L assemblage.[19] Both the L–B and L-b-L technique rely on electrostatic attraction between the negatively charged clay mineral layers and positively charged, but water-insoluble, molecules such as surfactants, dyes, and proteins. However, hybrid L–B films have also been prepared from dilute aqueous clay mineral dispersions and water-soluble alkylammonium cations.[20] This indicates that the rate of electrostatic attraction between clay mineral layers and alkylammonium cations is faster than the dissolution rate of the latter in the aqueous subphase of the L–B trough.

In this paper we make use of this fast formation of hybrid L–B films consisting of clay mineral layers and cationic surfactant molecules at the air–water interface to prepare hybrid layers of three components: clay mineral layers, cationic surfactants, and a cationic protein lysozyme. Firstly, the hybrid L–B film of clay mineral layers and surfactant molecules was formed at the air–water interface. Then lysozyme was introduced and allowed to interact with this hybrid film. The three-component hybrid L–B film was then transferred onto suitable substrates and characterized by AFM and spectroscopic techniques.

Results and Discussion

Two methods were used to prepare the clay–surfactant–protein L–B films. In method I, a clay–surfactant L–B film was first formed at the air–water interface of a dilute aqueous clay dispersion in the L–B trough. Then an aqueous solution of lysozyme was injected into the subphase from the back side of the barrier (see Scheme 1a). Method II is similar to method I except that the lysozyme solution was gently spread onto the clay–surfactant L–B film (Scheme 1b). The obtained L–B films are denoted surfactantclayLys-m*n*-*x*. The surfactants are ODAH (octadecylammonium cations) and RhB18 (octadecyl ester of rhodamine B). The clay minerals are saponite (sap) and Laponite (lap) and Lys stands for lysozyme. The method of introduction of lysozyme is denoted m1 or m2 for methods I or II, respectively, and x is the concentration of clay mineral in the subphase in $mg\,L^{-1}$.

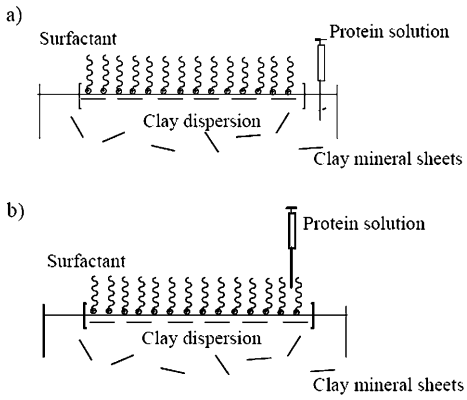

Scheme 1. Scheme of methods I (a) and II (b) for adding lysozyme solutions to the preformed clay–surfactant L–B films at the air–water interface.

Surface pressure versus time studies: The surface pressure was monitored as a function of time (π–t) at initial surface pressures of 0 and $10\,mN\,m^{-1}$ for three situations: 1) a surfactant monolayer over the subphase H_2O; 2) a surfactant monolayer over a clay dispersion (saponite: $10\,mg\,L^{-1}$; laponite: $2\,mg\,L^{-1}$), and 3) a hybrid L–B film of surfactant–clay over a clay dispersion. In the third case lysozyme was introduced according to methods I and II. At $\pi = 0\,mN\,m^{-1}$, the monolayer was not compressed and the surface pressure was monitored with time. At $\pi = 10\,mN\,m^{-1}$, the monolayer was compressed until a surface pressure of $10\,mN\,m^{-1}$ was obtained. The system was allowed to attain a constant area and then the π–t curves were recorded with and without addition of lysozyme.

Typical data are shown in Figure 1. In all cases studied, the surface pressure slowly decreases with time for monolayers of surfactant only and for hybrid L–B films of surfactant–clay and surfactant–clay–Lys. The rate of decrease of the surface pressure follows the order of ODAH < ODAH–clay–Lys < ODAH–clay. In the case of surfactant, the slight decrease of surface pressure with time is explained by the dissolution of surfactant molecules in the subphase.[20a] In the presence of clay, this decrease is more pronounced at either initial surface pressure of 0 or $10\,mN\,m^{-1}$. This indicates that the hybrid surfactant–clay layers are slowly dispersed in the subphase. The surfactant–clay–Lys films prepared by either method I or II follow the same trend with a rate of surface pressure decrease between those of the surfactant monolayer and of the surfactant–clay L–B film. The difference between method I and II is small but we observed systematically that the surface pressure decrease of method II is somewhat slower than that of the films prepared with method I.

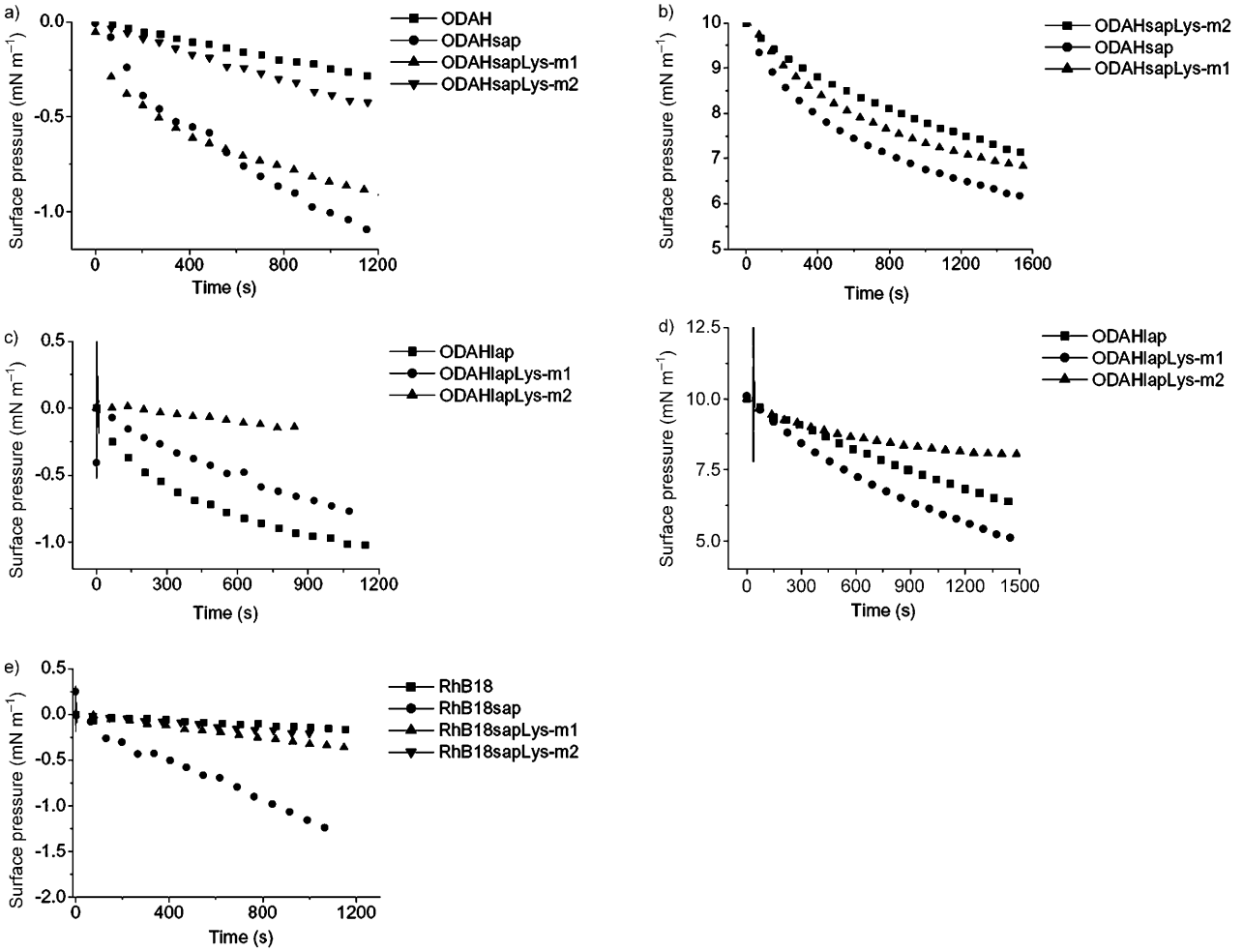

Figure 1. Surface pressure versus time (π–t) plots of the L–B films at the initial starting surface pressures of 0 and 10 mN m^{-1}: a) ODAHsap series at 0 mN m^{-1}; b) ODAHsap series at 10 mN m^{-1}; c) ODAHlap series at 0 mN m^{-1}; d) ODAHlap series at 10 mN m^{-1}; e) RhB18sap series at 0 mN m^{-1}. The initial vertical disturbance lines of the π–t plots is caused by the addition of lysozyme.

RhB18 forms a much more stable monolayer at the air–water interface than ODAH. The surface pressure remains fairly constant with time except for RhB18–saponite. The conclusion of these experiments is that surfactant–clay L–B films are not stable and slowly lose clay layers hybridized with surfactant cations in the subphase. With the introduction of lysozyme, this phenomenon is stopped or at least slowed down. The π–t curves also indicate that a constant surface pressure is not reached after 1000 s. We chose 15 min (900 s) as a standard waiting time before the start of compression of the L–B film.

Surface pressure versus area isotherms: Figure 2 gives the surface pressure versus area (π–A) isotherms of three types of L–B films: 1) surfactant (ODAH, RhB18); 2) hybrid L–B films of two components (ODAH–Lys, ODAH–clay, and RhB18–clay), and 3) hybrid L–B films of three components: surfactant, clay, and lysozyme. The minimum lift-off areas (MLA) of ODAH and RhB18 are 0.21 and 1.70 nm^2, respectively, and the apparent compressibilities are 3.9 and 30.7 m N^{-1} (see Table 1). These numbers are in agreement with the published data and reflect the liquid-expanded states of these L–B films (Figure 2a, e).[21] The addition of lysozyme to the ODAH monolayer only induces minor changes in the π–A isotherms. The MLA decreases slightly from 0.21 to 0.19 nm^2, but this falls within the limits of experimental accuracy. The same holds for the MLA of RhB18, but in this case the apparent compressibilities decrease upon addition of lysozyme to the RhB18 monolayer (see Table 1). For hybrid L–B films of three components the π–A isotherms of ODAH fall into four categories depending on the amount of clay in the subphase: 0.5, 5–10, 25, and 50–100 mg L^{-1} for saponite and into three categories 0.5, 2–5, and $\geq$10 mg L^{-1} for laponite (Figure 2a–d). With 0.5 mg L^{-1} saponite or laponite the three-component L–B films behave very similarly to the two-component L–B films. MLAs and apparent compressibilities are quite similar, especially in case of saponite (see Table 1). The second set of isotherms is obtained on subphases containing 5–10 mg L^{-1} saponite (Figure 2a and b). These isotherms are characterized by MLAs of 0.26–0.32 nm^2 and apparent compressibilities of 8.9–15.0 m N^{-1}. The addition of lysozyme to the

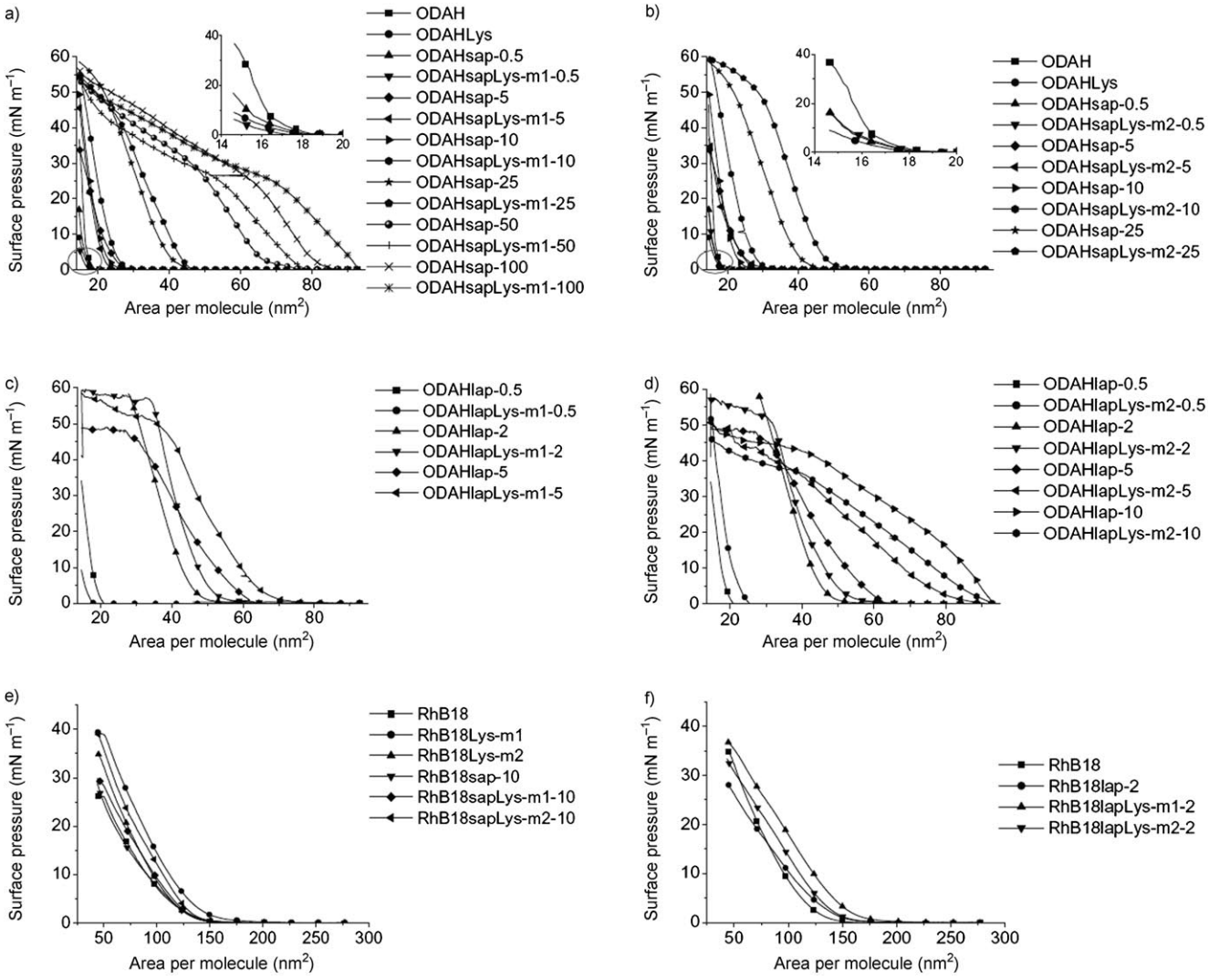

Figure 2. π–A isotherms for L–B films of ODAH (a, b, c, and d) and RhB18 (e, f) on clay dispersions of different concentrations with and without lysozyme. Insets in Figure 2a and b are the enlarged profiles of the circled area.

hybrid ODAH–sap L–B films leads to a small but systematic increase of the MLAs. The third set of three-component isotherms are obtained on subphases with 25 mg L^{-1} saponite or 2–5 mg L^{-1} laponite. The isotherms have similar MLAs and similar compressibilities: 0.45–0.55 nm^2 for saponite versus 0.50–0.60 nm^2 for laponite and 8.7–11.2 m N^{-1} for saponite and 7.2–11.3 m N^{-1} for laponite. Finally, at the highest clay concentrations in the subphase ($\geq$50 mg L^{-1} saponite; $\geq$10 mg L^{-1} laponite), the π–A isotherms all rise around the same MLA of 0.85–0.90 nm^2. This indicates that no stable "quasi-equilibrium" state film was obtained at the air–water interface before the start of compression.

With RhB18 as surfactant the π–A isotherms of the three-component systems are very similar to those of the two-component L–B films and that of RhB18 in terms of MLA and apparent compressibilities (Figure 2e, f; Table 1). The addition of lysozyme results in a small increase of the MLA values, which is more pronounced for laponite than for saponite. It also leads to a small but systematic decrease of the apparent compressibilities.

Characterization of the L–B films

UV-visible spectroscopy: To directly observe and to quantify lysozyme incorporated into the L–B films, mono- and multilayer films were deposited on quartz slides and monitored with UV-visible spectroscopy. The measured absorbance is due to the combination of scattering by the clay layers and absorption by the protein molecules in the film. For $\geq$250 nm the light scattering due to clay layers is almost independent of the wavelength. We therefore corrected the lysozyme spectra by subtracting the absorbance at 340 nm, which is only due to clay scattering. The spectra obtained are shown in Figure 3. Figure 3a displays the UV-visible spectra of the (ODAHsapLys-m1)$_n$ (n=1, 3, 5, 7, 9, 17, and 27) multilayers in the 340–190 nm range. The 270 nm band,

Table 1. Minimum lift-off area (MLA)[a] and apparent compressibility (C')[b] obtained from the π–A isotherms of Figure 2.

Sample [mg L^{-1}]	Method	Clay [mg L]	MLA [nm^2]	Δ(MLA) [nm^2][c]	C' [m N^{-1}]
ODAH	–	–	0.21	–	3.9
ODAHLys	I	–	0.19	−0.02	–
	II	–	0.19	−0.02	–
ODAHsap	–	0.5	0.19	−0.02	–
ODAHsapLys	I	0.5	0.18	−0.03	–
	II	0.5	0.19	−0.02	–
ODAHsap	–	5	0.27	0.06	13.2
ODAHsapLys	I	5	0.27	0.06	8.9
	II	5	0.32	0.11	15.0
ODAHsap	–	10	0.26	0.05	9.4
ODAHsapLys	I	10	0.30	0.09	10.2
	II	10	0.32	0.11	9.0
ODAHsap	–	25	0.45	0.24	10.3
ODAHsapLys	I	25	0.47	0.26	11.2
	II	25	0.55	0.34	8.7
ODAHlap	–	0.5	0.21	–	7.3
ODAHlapLys	I	0.5	0.18	−0.03	–
	II	0.5	0.21	0.01	9.4
ODAHlap	–	2	0.50	0.29	7.2
ODAHlapLys	I	2	0.57	0.36	8.4
	II	2	0.60	0.39	5.9
ODAHlap	–	5	0.52	0.31	7.8
ODAHlapLys	I	5	0.60	0.39	7.8
	II	5	0.60	0.39	11.3
ODAHlap	–	10	0.63	0.42	17.2
ODAHlapLys	I	10	0.75	0.54	14.8
	II	10	0.89	0.68	20.0
RhB18	–	–	1.70	–	30.7
RhB18Lys	I	–	2.01	0.31	22.1
	II	–	1.71	0.01	24.6
RhB18sap	–	10	1.72	0.02	33.8
RhB18sapLys	I	10	1.73	0.03	28.8
	II	10	1.75	0.03	24.7
RhB18Lap	–	2	1.82	0.12	32.8
RhB18LapLys	I	2	2.08	0.38	23.7
	II	2	1.94	0.24	25.9

[a] The minimum lift-off area (MLA) is defined as the molecular area at which the surface pressure starts to rise from zero. [b] The apparent compressibility is defined as $C' = -\frac{1}{A_{10}}\frac{A_{20}-A_{10}}{\pi_{20}-\pi_{10}}$, in which A_{10} and A_{20} correspond to the area per molecule at surface pressures of 10 (π_{10}) and 20 mN m^{-1} (π_{20}), respectively. [c] ΔMLA = MLA-(measured) − MLA(surfactant).

which originates from the π–π* transition of aromatic amino acid residues,[22] was used to quantify the amount of lysozyme incorporated in the films. The absorbance at 270 nm (inset of Figure 3a) is linearly proportional to the number of layers. From this observation the average amount of lysozyme deposited in one layer was calculated according to the method of Szabó et al.[19] The assumption was made that the extinction coefficient (ε) of lysozyme in the film equals that in solution. The latter is determined to be 950 m^2 kg^{-1} (see the Supporting Information, Figure S1). The calculated amount of protein deposited per mm^2 (n_S) and the average surface area per molecule (Ω) of lysozyme deposited in the L–B films are listed in Table 2. For the first layer, that is, $(ODAHsapLys)_1$, the average amount of lysozyme is approximately 1.3 ng mm^{-2} and the surface area per molecule (Ω) is (18.2 ± 3.0) nm^2. For the multilayer film $(ODAHsapLys)_n$, the average amount of lysozyme is (1.0 ± 0.1) ng mm^{-2}. These numbers agree well with the 1.4 ng mm^{-2} of Szabó et al. for L-b-L multilayers.[19]

The spectra of the hybrid films $(ODAHlapLys\text{-}m1)_n$ (n = 1, 3, 5, 7, 9, 11, 13, and 15) are shown in Figure 3b. The 270 nm band of lysozyme is barely visible. It starts to rise above the background after 15 multilayers. If the absorbance of 15 multilayers is used, the amount of lysozyme per layer is approximately 0.4 ng mm^{-2}. This must be considered as the detection limit.

To confirm that the ODAH–clay L–B film can adsorb lysozyme, we also performed adsorption experiments in an aqueous clay dispersion. The data are shown in Table S1 in the Supporting Information. With the amount of lysozyme introduced equal to the theoretical cation exchange capacities (CEC), the amount adsorbed is 7.1–8.3 % of the CEC, independent of the amount of ODAH. These data show that lysozyme can be adsorbed on a clay presaturated with ODAH, the amount adsorbed being in the range 7.1–8.3 % of the CEC. With 2.7 wt % of the clay or 0.27 mg in the hybrid L–B film (see the Supporting Information) the amount of adsorbed lysozyme is then 40–240 μg of lysozyme in the three-component L–B films.

Attenuated total reflectance (ATR) FTIR spectroscopy: Typical ATR-FTIR spectra of L–B films are given in Figure 4a. They are compared with the spectra of saponite and laponite films, which were prepared by immersing the ZnSe internal reflection element (IRE) in 10 mg L^{-1} saponite and 2 mg L^{-1} laponite dispersions, respectively, for 10 min. The clays have the typical bands of Si−O in-plane and out-of-plane stretching vibrations at 1000 and 1064 cm^{-1}, respectively. They are observed for all the L–B films with saponite and laponite, thus confirming the presence of clay layers in these films. If the films contain lysozyme, the Si−O stretching bands overlap with vibrations of the protein. The band at 1640 cm^{-1} is the deformation vibration of the water molecules in the films.[23] This band might be present in all films, but it overlaps with the amide I band of lysozyme and some vibrations of ODAH. As seen in Figure 4a, ODAH vibrations are not easily distinguished from vibrations of lysozyme. However, in the hybrid two-component films (ODAHsap, ODAHlap) a typical C=O vibration is observed at 1740 cm^{-1}. This band is indicative of partial conversion of ODAH to the corresponding carbamate, due to reaction with dissolved CO_2 and methanol (or ethanol), always present in chloroform to stabilize the latter. The reaction has been observed by Ras et al.[24] The second characteristic band of ODAH is the CH_2 antisymmetric stretch at 2912 cm^{-1} in the ODAH monolayer. This band shifts to 2924 cm^{-1} for hybrid L–B films. This shift is indicative for a transition of ordered alkyl chains in the ODAH monolayer to disordered alkyl chains in the hybrid films, that is, when ODAH is adsorbed on the surface of the clay layers.[25]

The films of lysozyme and the corresponding three-component hybrid films including saponite and laponite have the typical amide I and II bands around 1658 and 1540 cm^{-1},

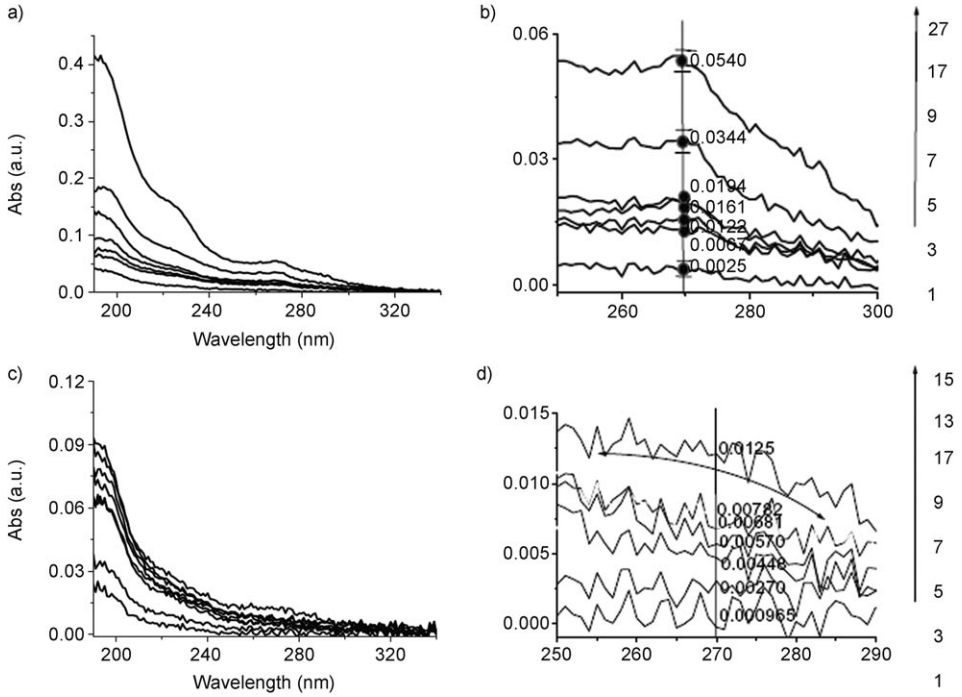

Figure 3. UV-visible spectra of the hybrid films a) $(ODAHsapLys\text{-}m1)_n$ and c) $(ODAHlapLys\text{-}m1)_n$ on quartz slides prepared by vertical deposition (the arrow and accompanying numbers on the right indicate the number of layers, n) at 20 mN m^{-1} from 10 mg L^{-1} saponite and 2 mg L^{-1} laponite, respectively. b,d) Show the enlarged spectra around 270 nm.

Table 2. Amounts (n_S) and surface area per molecule (Ω)[a] of lysozyme deposited in ODAHsap films; percentage of saponite at the interface (% Clay);[b] and percentage of lysozyme adsorbed by the saponite layer at the air–water interface (% Lys).[b]

Sample	n_S [ng mm^{-2}]	Ω [nm^2]	% Clay	% Lys
$(ODAHsapLys\text{-}m1)_1$	1.3 ± 0.2	18.2 ± 3.0	2.7	0.5–0.68
$(ODAHsapLys\text{-}m1)_n$[c]	1.0 ± 0.1	22.7 ± 2.0	–	–
$(ODAHsapLys\text{-}m2)_1$	1.4 ± 0.2	17.8 ± 3.0	2.7	0.68–0.92
$(ODAHsapLys\text{-}m2)_n$[c]	1.0 ± 0.1	22.7 ± 2.0	–	–

[a] Calculation method is given in ref. [19], and an example of the calculation of the ODAHsapLys film is given in the Supporting Information. [b] An example of the calculation of % Clay and % Lys is presented in the Supporting Information. [c] The average value for one hybrid layer in the film.

respectively. In some cases a weak 1740 cm^{-1} band is reminiscent of the presence of carbamate, but this is much less than in the absence of protein. The amide I ($\approx$1658 cm^{-1}) band is mainly due to C=O stretching vibrations. The frequency of the amide I band depends on the secondary structure of the protein.[26] The deconvolution is performed with Gaussian band shapes at fixed frequencies. The results are shown in Figure 4b for the region 1485–1765 cm^{-1}. In the film of lysozyme the band maximum is at 1658 cm^{-1} and four components are resolved at 1632 (antiparallel β sheets), 1640 (H_2O), 1658 (α helices), and 1682 cm^{-1} (β turns with a contribution of COCOOH stretching modes of −COOH in acidic amino acids).[27] In the presence of saponite and laponite, that is, ODAHsapLys and ODAHlapLys, five components are present. A band at 1620 cm^{-1} becomes apparent, which is ascribed to intermolecular antiparallel β-sheet aggregation.[28] This reveals that there are lysozyme aggregates in ODAHsapLys and ODAHlapLys films. The intensities of $\nu_{as}(CH_2)$ (2924 cm^{-1}) and $\nu_s(CH_2)$ (2851 cm^{-1}) in ODAHclayLys are weaker than in the ODAHclay films. This result indicates that the density of ODAH molecules is lower in ODAH–clay–Lys film than in ODAH or ODAH–clay film.[29] It is reasonable to suppose that some ODAH was replaced by protein and dissolved into the subphase.

AFM: Figure 5a and b display the AFM images in topography and cantilever deflection mode of an L–B film of ODAHsap obtained by horizontal deposition on a glass substrate at a

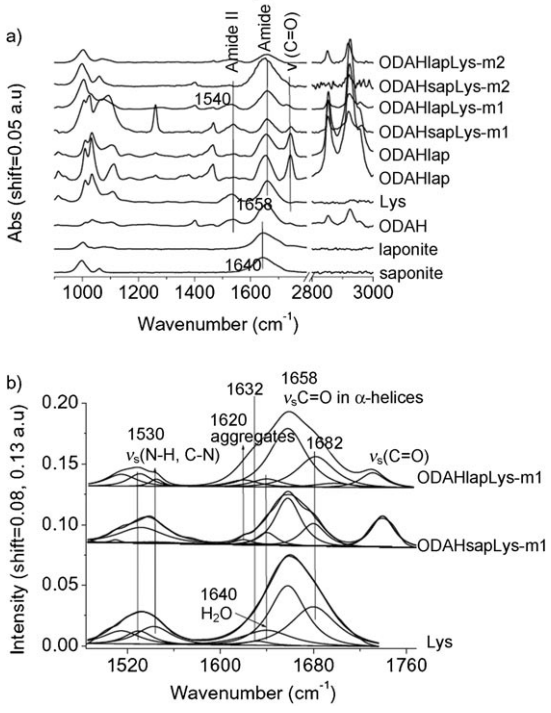

Figure 4. a) ATR-IR absorbance spectra of saponite, laponite, and lysozyme deposited by immersion of the ZnSe IRE in the diluted solutions; and L–B films of ODAH and the hybrid films involving clays and lysozyme prepared by vertical deposition from 10 mg L^{-1} saponite or 2 mg L^{-1} laponite at 20 mN m^{-1}; b) Deconvoluted ATR-IR spectra of lysozyme, ODAHsapLys-m1, and ODAHlapLys-m1.

surface pressure of 2 mN m^{-1}. The figures show randomly oriented saponite layers of various sizes and shapes. Some are single layers, that is, they have a height of approximately 1.3 nm (see the arrows in Figure 5a), others are aggregates with a height up to 10 nm (pink areas in Figure 5a). Figure 5c and d show AFM images in topography and cantilever deflection mode of a ODAHsapLys-m1 film on a glass substrate. We observe similar randomly oriented saponite layers and bean-shaped granules, some on the saponite layers, and some in the space between the saponite layers. Most of these granules have a width of approximately 20 nm and a height less than 10 nm. We interpret these bean-shaped granules as aggregates of lysozyme molecules. Individual lysozyme molecules are not resolved. Figure 5e gives the height analysis along the line in Figure 5c. The arrows indicate substrate, saponite layers, and saponite layer+lysozyme. The typical thicknesses of a single saponite layer of 1.3 nm and of an isolated protein granule of 4.5 nm were measured (Figure 5c and e). Figure 5f gives the cantilever deflection mode of the ODAHsapLys-m1 film deposited at 20 mN m^{-1}. At this tenfold higher surface pressure the saponite layers are more densely packed, and the pink areas are indicative of some larger lysozyme aggregates. We also found that some of the lysozyme aggregates are aligned in straight lines from upper left to lower right. This linear assemblage of lysozyme was confirmed at different scanning angles under AFM. Clearly, this linear assemblage was formed under the higher pressure. In the case of laponite, a dense layer of laponite particles is observed (see Figure S2a, b in the Supporting Information). If lysozyme is added (see Figure S2c, d in the Supporting Information) the laponite particles become less discernable. We do not clearly see lysozyme aggregates. Some pink spots are visible, but whether they are due to aggregates of laponite layers or of lysozyme molecules remains an open question. In agreement with the analysis by UV-visible spectroscopy, the amount of lysozyme in ODAHlapLys film is lower than that of ODAHsapLys. This is confirmed by the observation of less lysozyme granules in the ODAHlapLys film.

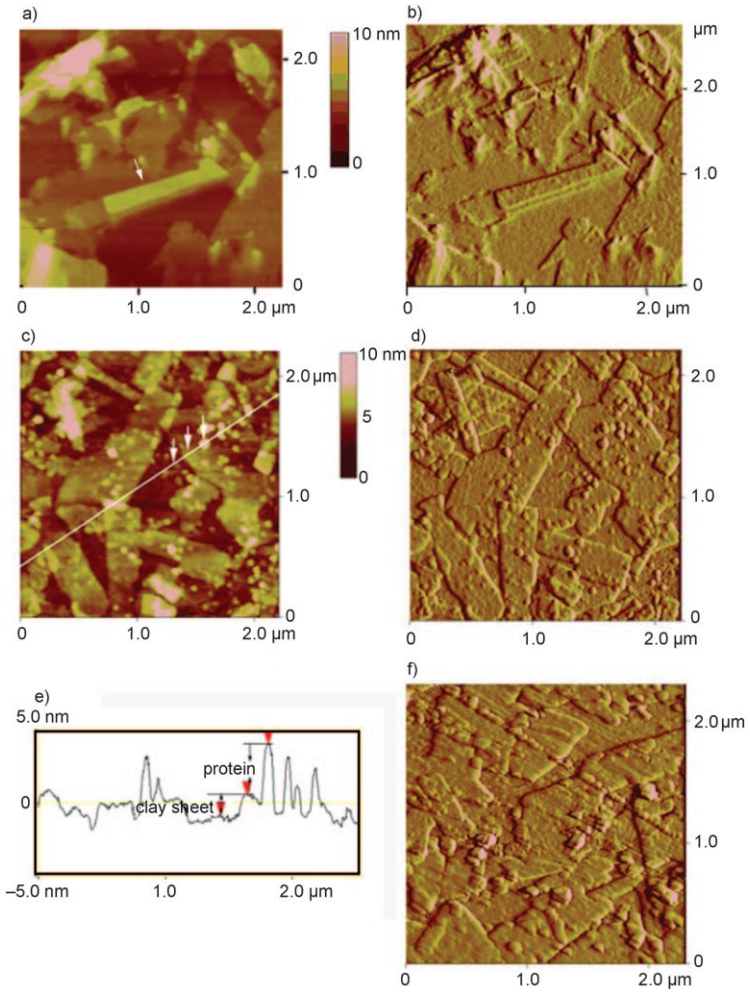

Figure 5. AFM images of the prepared L–B films transferred onto glass substrates at 2 mN m^{-1} unless specified. a),b) topographical and cantilever deflection mode of ODAHsap obtained in contact mode; c) topographical image of ODAHsapLys-m1; d) cantilever deflection mode of ODAHsapLys-m1; e) the height profiles along the line in Figure 5c; f) cantilever mode of ODAHsapLys-m1 deposited at 20 mN m^{-1}.

Figure S2e is the AFM image for an ODAHsapLys film that was prepared at 2 mN m^{-1} by means of method II (see the Supporting Information). This film shows a more homogeneous morphology than that of the films prepared by method I (Figure 5c). Figure S2f gives the height analysis along the line in Figure S2e, and the pink spots on the saponite layer have a height of 4.1 nm, due to aggregates of lysozyme molecules (see the Supporting Information). In L–B films that were prepared with RhB18 as surfactant over a saponite dispersion (see Supporting Information, Figure S3), bean-shaped protein granules were also found (RhB18sapLys). This can be observed by comparison of the AFM images of RhB18sapLys in Figure S3d, f and RhB18sap in Figure S3a, c in the Supporting Information. Figure S3b, e gives the height analysis along the lines displayed in Figure S3a, d, respectively. The lysozyme aggregates denoted by the arrows in Figure S3e are around 5.2 nm in height. The RhB18 hybrid films prepared over laponite dispersion are characterized by a dense layer of laponite particles (Figur-

e S3g, i). Upon addition of lysozyme in the RhB18Lap films, the density of the laponite particles seems to be lower and the films are rougher. The height analysis along the line displayed in Figure S3j indicates particles with a height of 4.65 nm, which are assigned to aggregates of lysozyme molecules.

Conclusion

Three-component hybrid films of surfactant (ODAH, RhB18), clay minerals (saponite, laponite), and lysozyme have been prepared by the L–B technique. The presence of the three components in the films were confirmed directly by AFM, UV-visible, ATR-FTIR spectroscopy, and indirectly by the π–A isotherms. In the hybrid L–B films, saponite forms a layer of randomly oriented elementary layers of various sizes and shapes. Laponite forms a film of densely packed layers. At the air–water interface ODAH is partially oxidized to carbamate as reported before.[24] The amount of carbamate is highest for the two-component hybrid films, that is, ODAHsap and ODAHlap, and much less in the three-component film with lysozyme. This might indicate that lysozyme preferentially replaces the neutral carbamate molecules in the hybrid films instead of the cationic, and therefore more strongly bound, ODAH.

It is remarkable that the water-soluble lysozyme molecules are incorporated in the preformed ODAH–clay films at the air–water interface, even when the lysozyme solution is injected in the subphase (method 1). Only a minor fraction of the clay layers in the subphase (2.7%) are taken up in the hybrid film at the air–water interface and lysozyme molecules are expected to exchange on the clay layers in the subphase and in the hybrid film at the air–water interface. Besides this exchange, the observation of lysozyme molecules in the hybrid films can also be the result of two additional phenomena: 1) exchange of lysozyme–clay layers of the subphase with ODAH–clay layers at the air–water interface; 2) lysozyme molecules spontaneously aggregate at the air–water interface, independently of the presence of ODAH–clay layers at the air–water interface. The latter is supported by the observation of lysozyme aggregates in the AFM images that are not adsorbed on clay layers (Figure 5). The implications are that 1) it must be possible to construct lysozyme–clay films with the L–B technique in the absence of surfactant molecules; and 2) L–B films of lysozyme can be constructed in the absence of clay layers and of surfactants. This will be the subject of future publications.

Experimental Section

Materials: The clays used in this study were saponite ($[(Si^{4+}_{3.57}Al^{3+}_{0.38}Fe^{3+}_{0.05})(Mg^{2+}_{3.00})O_{10}(OH)_2]M^{+}_{0.43}$) obtained from the Source Clays Repository of the Clay Minerals Society and laponite ($[(Si^{4+}_{4.00})(Mg^{2+}_{2.67}Li^{+}_{0.33})O_{10}(OH)_2]Na^{+}_{0.33}$) of RD grade purchased from Laporte Inorganics, UK. Their theoretical cation-exchange capacities (CEC) were 0.74 and 0.57 mmol Na^+ per gram, respectively.[30] Stock dispersions of saponite and laponite were prepared by dispersing the clay minerals (1.000 g) in millipore (MQ) water (1000 mL, 18.2 MΩ). The dispersion was diluted to a predefined concentration with MQ water and stirred for 24 h before use. Lysozyme (Lys, from chicken egg white; $M_r = 14\ 300$ Da; E.C. 3.2.1.17; size $3\times3\times3.5$ nm; isoelectric point: 11.1)[31] was purchased from Sigma. Octadecylammonium chloride ($ODAH^+Cl^-$) was synthesized by reaction of the corresponding amine with hydrochloric acid. The ammonium salt was recrystallized in ethanol twice. Quartz, glass, and ZnSe crystals were used to deposit L–B films. Quartz (12×61 mm) was used for UV/Vis absorbance spectroscopy. Glass platelets were used as supports for AFM, and the ZnSe crystal (45° trapezoidal crystals $50\times20\times2$ mm, Spectroscopy Central, UK) served as the internal reflection element (IRE) for ATR-FTIR spectroscopy. Quartz slides and glass slides were cleaned by sonication in a detergent solution. Then they were put in chromic acid for at least 20 min to remove surfactants, followed by cleaning in piranha solution (mixture of H_2SO_4 (98%)/H_2O_2 (35%) with a ratio of 7:3, v/v) for 30 min at 90°C. The substrates were then extensively rinsed with MQ water, dried under a stream of nitrogen (99.99%), and immediately used for the film deposition. Hydrophobic slides were prepared from the above-treated slides by heating them at reflux with phenyltrimethoxysilane in toluene (5.0 g L^{-1}) under a nitrogen atmosphere for 48 h. After the reaction, the hydrophobic glass was washed with toluene and diethyl ether and dried in a nitrogen flow. The surface was again rinsed with water several times and then dried in air. ZnSe IRE was cleaned by polishing it with a slurry of cerium oxide followed by rinsing it with copious amounts of MQ water.

L–B film preparation: A Langmuir–Blodgett trough (Nima, model 611) was used for the preparation of the films. This system uses a pair of mobile barriers for compressing the monolayer at the air–water interface and a Wilhelmy balance for measuring the interfacial pressure. The system was operated in air at room temperature (25°C). The hybrid films were prepared on dilute clay dispersions. A microsyringe was used to spread the $ODAH^+Cl^-$ (200 μL) dissolved in chloroform + methanol (0.137 mg mL^{-1}, 0.45 mmol L^{-1}, chloroform/methanol 19:1, v/v) over the air–water interface. After the $ODAH^+Cl^-$ solution had been spread, the solvent was allowed to evaporate for 15 min, and a floating film of ODAH hybridized with the clay mineral sheets was formed.

***π–t* curves**: Lysozyme aqueous solutions (1.0 mL, 5.6×10^{-4} M) were added into the clay dispersion of the L–B trough. The surface pressure was recorded while the system was allowed to equilibrate with fixed barriers. Two initial starting surface pressures (0 and 10 mN m^{-1}) were applied. At the initial surface pressure of 0 mN m^{-1}, the barrier was fixed at the maximum area (500 cm^2). π–t curves were recorded immediately after protein injection with the surface pressure reset to 0 mN m^{-1}. In the case of 10 mN m^{-1}, the area was first compressed to obtain a surface pressure of 10 mN m^{-1} before it was fixed. The lysozyme solution was added and π–t curves were recorded.

***π–A* isotherms and film preparation**: The surface pressure versus area (π–A) isotherms were recorded 15 min after injection of the lysozyme solution. All L–B films were compressed at a rate of 20 $cm^2 min^{-1}$ at room temperature. Films were prepared by vertical or horizontal deposition at the desired surface pressure. For vertical deposition, hydrophilic slides were dipped into the subphase before surfactant spreading. A film was deposited in an upstroke at a desired surface pressure. In the case of horizontal deposition, the hydrophobic substrates were allowed to approach the hybrid films at the air–water interface and were kept there for 10 min while the surface pressure remained at the preset pressure. Multilayer films were prepared by repeating the procedures as explained above.

Characterization

UV/Vis spectroscopy: To obtain the extinction coefficients of the proteins at 270 nm, the absorbance of lysozyme solutions with known concentration were measured in quartz cuvettes at 270 nm. A linear relation was obtained between lysozyme concentrations and absorbance. The extinction coefficient (ε) of lysozyme was calculated according to the Lambert–Beer law. Spectra of the quartz slides were also recorded and subtracted from the UV/Vis spectra of the as-prepared L–B films. A Cary 5 UV-Vis-NIR spectrophotometer (Varian, Palo Alto, CA, USA) was used. The wavelength resolution was 1.0 nm.

ATR-FTIR spectroscopy: ATR-FTIR spectra were collected on a Bruker IFS 66v/s spectrometer. Films were vertically deposited on ZnSe IRE in the L–B trough. The spectra were registered between 4000 and 400 cm^{-1} with 128 scans per spectrum at an established standard resolution of 4 cm^{-1}. The 1486–1770 cm^{-1} region was smoothed with a 10-point Savitzky–Golay function. The components of the amide I and II bands were determined by using an iterative least-squares Levenberg–Marquardt algorithm (OPUS spectroscopy software). The individual components were obtained with Gaussian band shapes. The frequencies were kept constant during deconvolution; only band height and band width were allowed to change.

AFM: AFM measurements were performed on a Multimode atomic force microscope with a Nanoscope IIIa control system (Digital Instruments, Santa Barbara, CA) at ambient temperature. A 10 μm scanner with a Si_3N_4 tip (Veeco NanoProbe NP-20, narrower long cantilever) with spring constant (0.032 $mN\,m^{-1}$) was used for operation in the contact mode. The topographs were processed (background substraction with standard "roll ball" algorithm and subsequent second-order plane leveling) and analyzed (line and area analysis) by using the Nanoscope III V5.12r2 software.

Acknowledgements

This research was financially supported by the IAP. The authors are grateful to Willem Vanderlinden for assisting with AFM measurements. S.D.M. acknowledges a postdoc grant from the K.U. Leuven. The authors are grateful for Long Term Structural Funding: Methusalem Funding by the Flemish Government.

[1] J. Stubbe, W. A. van der Donk, *Chem. Rev.* **1998**, *98*, 705.
[2] C. V. Kumar, A. Chaudhari, *J. Am. Chem. Soc.* **2000**, *122*, 830.
[3] a) P. N. Bryan, *Chem. Rev.* **2002**, *102*, 4805; b) Y. Lu, S. M. Berry, T. D. Pfister, *Chem. Rev.* **2001**, *101*, 3047; c) L. Gorton, G. Marko-Varga, E. Dominguez, J. Emneus, *Analytical Applications of Immobilized Enzyme Reactor*s (Eds.: S. Lam, G. Malikin), Blackie Academic & Professional, New York, **1994**, p. 1.
[4] a) *Physical Chemistry of Biological Interface* (Eds.: A. Baskin, W. Norde, M. Dekker), Marcel Dekker, New York, **1999**; b) W. Senaratne, L. Andruzzi, C. Ober, *Biomacromolecules* **2005**, *6*, 2427; c) C. Czeslik, *Z. Phys. Chem.* **2004**, *218*, 771.
[5] L. He, A. F. Dexter, A. P. J. Middelberg, *Chem. Eng. Sci.* **2006**, *61*, 989.
[6] D. Avnir, D. Levy, R. Reisfeld, *J. Phys. Chem.* **1984**, *88*, 5956.
[7] P. Labbé, B. Brahimi, G. Reverdy, C. Mousty, R. Blankespoor, A. Gautier, G. J. Deraud, *Electroanal. Chem.* **1994**, *379*, 103.
[8] *Protein Architecture: Interfacing Molecular Assemblies and Immobilization Biotechnology* (Eds.: Y. Lvov, H. Mohwald), Marcel Dekker, New York, **1999**.
[9] a) I. Langmuir, *J. Am. Chem. Soc.* **1917**, *39*, 1848; b) K. B. Blodgett, *J. Am. Chem. Soc.* **1935**, *57*, 1007; c) D. Y. Takamoto, E. Aydil, J. A. Zasadzinski, A. T. Ivanova, D. K. Schwartz, T. Yang, P. S. Cremer, *Science* **2001**, *293*, 1292; d) D. J. Shaw, *Introduction to Colloid and Surface Chemistry*, Butterworth & Co., London **1980**.
[10] a) O. Albrecht, K. Sakai, K. Takimoto, H. Matsuda, K. Eguchi, T. Nakagiri, *Mol. Biomol. Electron.* **1994**, *240*, 341; b) X. Chen, S. Lenhert, M. Hirtz, N. Lu, H. Fuchs, L. Chi, *Acc. Chem. Res.* **2007**, *40*, 393; c) X. Li, L. Zhang, X. Wang, I. Shimoyama, X. Sun, W. S. Seo, H. Dai, *J. Am. Chem. Soc.* **2007**, *129*, 4890; d) S. Paul, C. Pearson, A. Molloy, M. A. Cousins, M. Green, S. Kolliopoulou, P. Dimitrakis, P. Normand, D. Tsoukalas, M. C. Petty, *Nano Lett.* **2003**, *3*, 533; e) L. Caseli, A. C. Perinotto, T. Viitala, V. Zucolotto, O. N. Oliveira, Jr., *Langmuir* **2009**, *25*, 3057.
[11] a) C. L. Yan, Y. Lu, *Prog. Chem.* **2008**, *20*, 969; b) I. M. Pepe, C. Nicolini, *J. Photochem. Photobiol. B* **1996**, *33*, 191; c) L. Caseli, R. G. Oliveira, D. C. Masui, *Langmuir* **2005**, *21*, 4090.
[12] a) H. A. Rinia, R. A. Demel, J. P. J. M. van der Eerden, B. de Kruijff, *Biophys. J.* **1999**, *77*, 1683; b) M. Benz, T. Gutsmann, N. Chen, R. Tadmor, J. Israelachvili, *Biophys. J.* **2004**, *86*, 870; c) P. Lozano, A. J. Fernández, J. J. Ruiz, L. Camacho, M. T. Martín, E. Munõz, *J. Phys. Chem. B* **2002**, *106*, 6507; d) F. d'Acapito, I. Emelianov, A. Relini, P. Cavatorta, A. Gliozzi, V. Minicozzi, *Langmuir* **2002**, *18*, 5277.
[13] a) E. M. Clop, P. D. Clop, J. M. Sanchez, M. A. Perillo, *Langmuir* **2008**, *24*, 10950; b) P. L. Edmiston, J. E. Lee, S. S. Cheng, S. S. Saavedra, *J. Am. Chem. Soc.* **1997**, *119*, 560; c) M. Seufert, M. Schaub, G. Wegner, G. Wenz, *Angew. Chem.* **1995**, *107*, 363; *Angew. Chem. Int. Ed. Engl.* **1995**, *34*, 340.
[14] a) A. P. Girard-Egrot, S. Godoy, L. J. Blum, *Adv. Colloid Interface Sci.* **2005**, *116*, 205; b) S. P. Beier, A. D. Enevoldsen, G. M. Kontogeorgis, E. B. Hansen, G. Jonsson, *Langmuir* **2007**, *23*, 9341; c) T. Kamilya, P. Pal, G. B. Talapatra, *J. Phys. Chem. A* **2007**, *111*, 1199; d) M. J. Parry, J. M. I. Alakoskela, H. Khandelia, S. A. Kumar, M. Jäättelä, A. K. Mahalka, P. K. Kinnunen, *J. Am. Chem. Soc.* **2008**, *130*, 12953.
[15] L. Shen, N. Hu, *Biomacromolecules* **2005**, *6*, 1475.
[16] C. P. Michael, *Langmuir–Blodgett Films: An Introduction*, Cambridge University Press, Cambridge, **1996**, p. 127.
[17] C. Del Hoyo, *Applied Clay Science* **2007**, *36*, 103.
[18] R. H. A. Ras, Y. Umemura, C. T. Johnston, A. Yamagishi, R. A. Schoonheydt, *Phys. Chem. Chem. Phys.* **2007**, *9*, 918.
[19] T. Szabó, M. Szekeres, I. Dékány, C. Jackers, S. De Feyter, C. T. Johnston, R. A. Schoonheydt, *J. Phys. Chem. C* **2007**, *111*, 12730.
[20] a) Y. Umemura, A. Yamagishi, R. Schoonheydt, A. Persoons, F. De Schryver, *Langmuir* **2001**, *17*, 449; b) Y. Umemura, A. Yamagishi, R. Schoonheydt, A. Persoons, F. C. De Schryver, *Thin Solid Fims* **2001**, *388*, 5.
[21] a) E. F. Porter, *J. Am. Chem. Soc.* **1937**, *59*, 1883; b) J. J. Betts, B. A. Pethica, *Trans. Faraday Soc.* **1956**, *52*, 1581.
[22] O. H. Lowry, N. J. Rosenbrough, A. L. Farr, R. J. Randall, *J. Biol. Chem.* **1951**, *193*, 265.
[23] M. Xu, Y. S. Choi, Y. K. Kim, K. H. Wang, I. J. Chung, *Polymer* **2003**, *44*, 6387.
[24] R. H. A. Ras, C. T. Johnston, R. A. Schoonheydt, *Chem. Commun.* **2005**, 4095.
[25] R. H. A. Ras, Ph.D. Thesis, K. U. Leuven (Belgium), **2003**.
[26] W. Hammond, E. Prouzet, S. D. Mahanti, T. J. Pinnavaia, *Microporous Mesoporous Mater.* **1999**, *27*, 19.
[27] N. A. Nevskaya, Y. N. Chirgadze, *Biopolymers* **1976**, *15*, 637.
[28] a) N. Dermirdöven, C. M. Cheatum, H. S. Chung, M. Khalil, J. Knoester, A. Tokmakoff, *J. Am. Chem. Soc.* **2004**, *126*, 7981; b) Z. Ganim, H. S. Chung, A. W. Smith, L. P. DeFlores, K. C. Jones, A. Tokmakoff, *Acc. Chem. Res.* **2008**, *41*, 432.
[29] E. Pechkova, P. Innocenzi, L. Malfatti, T. Kidchob, L. Gaspa, C. Nicolini, *Langmuir* **2007**, *23*, 1147.
[30] B. Van Duffel, R. A. Schoonheydt, C. P. M. Grim, F. C. De Schryver, *Langmuir* **1999**, *15*, 7520.
[31] K. Kandori, S. Oda, S. Tsuyama, *J. Phys. Chem. A* **2008**, *112*, 2542.

Received: March 4, 2009
Published online: January 26, 2010

